

# Monte Carlo Simulation Study of Hot-Particle Detection in Voluminous Samples by Gamma Spectrometry

Liang T. Chu<sup>1,2</sup>, Adam G. Burn<sup>1,2</sup>, Clayton J. Bradt<sup>1</sup>, Thomas M. Semkow<sup>1,2</sup>

<sup>1</sup>Wadsworth Center, New York State Department of Health, Albany, NY, USA

<sup>2</sup>Department of Environmental Health Sciences, School of Public Health, University at Albany, State University of New York, Rensselaer, NY, USA

Email: thomas.semkow@health.ny.gov

**How to cite this paper:** Chu, L.T., Burn, A.G., Bradt, C.J. and Semkow, T.M. (2021) Monte Carlo Simulation Study of Hot-Particle Detection in Voluminous Samples by Gamma Spectrometry. *Journal of Applied Mathematics and Physics*, 9, 1522-1540.  
<https://doi.org/10.4236/jamp.2021.97104>

**Received:** June 9, 2021

**Accepted:** July 19, 2021

**Published:** July 22, 2021

Copyright © 2021 by author(s) and Scientific Research Publishing Inc.

This work is licensed under the Creative Commons Attribution International License (CC BY 4.0).

<http://creativecommons.org/licenses/by/4.0/>



Open Access

## Abstract

In this work, we addressed the inhomogeneity problem in gamma spectrometry caused by hot particles, which are dispersed into environment from large nuclear reactor accidents such as at Chernobyl and Fukushima. Using Monte Carlo simulation, we have determined the response of a gamma spectrometer to individual and grouped hot particles randomly distributed in a soil matrix of 1-L and 0.6-L sample containers. By exploring the fact that the peak-to-total ratio of efficiencies in gamma spectrometry is an empirical parameter, we derived and verified a power-law relationship between the peak efficiency and peak-to-total ratio. This enabled creation of a novel calibration model which was demonstrated to reduce the bias range and bias standard deviation, caused by measuring hot particles, by several times, as compared with the homogeneous calibration. The new model is independent of the number, location, and distribution of hot particles in the samples. In this work, we demonstrated successful performance of the model for a single-peak <sup>137</sup>Cs radionuclide. An extension to multi-peak radionuclide was also derived.

## Keywords

Chernobyl, Fukushima, Peak Efficiency, Total Efficiency, Signal Detection Theory

## 1. Introduction

In gamma spectrometry of environmental, food, and industrial matrices, voluminous samples are usually analyzed in quantities ranging from a fraction of to several L or kg. This is done in order to increase the sensitivity as well as to bet-

ter assess the extent of any contamination present. Germanium gamma detector (Ge) calibration for voluminous samples is accomplished with either the physical traceable standards or computational methods. Both types of calibrations assume homogeneous distribution of radioactivity in large samples, using bulk peak efficiency  $p_b$  of the Ge detector. In many types of samples, however, distribution of radioactivity may be heterogeneous. This can lead to substantial bias in activity determination.

One type of inhomogeneity may be referred to as geometrical, where different sections of the sample may have varied radionuclide activities. This has been investigated for spiked reference materials [1], where analysis of variance was used to determine homogeneity. Assumptions about geometrical inhomogeneity were studied in terms of cylinder and disc [2], fraction of volume not containing radiation [3], or two sections of Marinelli beaker [4] [5].

Another type of inhomogeneity can arise from sample granularity. It was shown, using Monte-Carlo (MC) simulation, that the Ge detector peak efficiency dropped with increased granularity [6]. However, this effect has not been seen experimentally for grains of soil or polystyrene much smaller than the container size, in which spiking solution occupied an interstitial space [7].

Yet another important type of inhomogeneity of interest to this investigation is due to suspension of “hot particles” in the sample matrix. The problem of hot particles was originated from nuclear detonation fallout [8] and was extensively observed and studied following the 1986 Chernobyl [9] [10] and 2011 Fukushima nuclear accidents [11] [12]. Hot particles from nuclear accidents are the results of several formation mechanisms: disintegration of nuclear fuel in the explosion and fires; condensation of liquid droplets; and deposition of volatile fission products such as Cs on fly ash and atmospheric aerosols [13]. The composition of hot particles depends on the formation mechanism. The Chernobyl particles can be mono-elemental, bi-elemental, or fuel fragments [13], whereas Fukushima particles contain predominately  $^{137}\text{Cs}$ , referred to as Cs microparticles [12]. Hot particles can have diameters from a fraction of a micrometer to over 100  $\mu\text{m}$  [14] and their size distribution is often assumed as lognormal [15] or arbitrary [16].

Hot particles travel significant distances with the plume [17] [18]. Gas-phase and aerosol  $^{131}\text{I}$  from Fukushima were observed as far as New York State [19]. Hot particles deposit on the ground and cause contamination of soil, water, crops, food, etc. Additional mechanisms for hot particle dispersion from nuclear accidents involve weathering of radioactive lava (melted fuel elements) [20] and sorption of ionic  $^{137}\text{Cs}$  on soil particles [21].

An entirely different source of hot particles, also referred to as discrete radioactive particles, is corrosion of neutron irradiated steel in normal nuclear reactor operation [22] as well as fuel reprocessing [23]. The presence of hot particles in potential dirty bomb explosions has been described [24].

The presence of hot particles in voluminous samples creates unusual chal-

allenges in gamma spectrometry regardless of their origin. There are several approaches to ameliorate these challenges, such as instrumental, radiochemical, and modeling. On the instrumental side, one can perform digital radiography to identify locations of hot particles [25]. Rotating waste drum scanning techniques can locate and determine heterogeneous distribution of radioactivity, utilizing emission/transmission measurements combined with modeling [26] [27] [28] [29] [30].

Among radiochemical methods, mechanical mixing only repositions hot particles in the sample without homogenization. Chemical homogenization of large samples is difficult. In addition, the particles formed as fuel elements, by condensation, or explosion are typically refractory and only high-temperature fusion [31] or HF digestion [32] can dissolve them. However, the ionic fraction, such as containing aerosol-deposited Cs and I, can be homogenized for some matrices as has been demonstrated for food using tetramethylammonium hydroxide and enzymes [33] [34].

A voluminous sample can contain both uniformly distributed radioactivity as well as inhomogeneous hot particles. It was estimated that at least 65% of total activity in the 30-km zone around Chernobyl was due to hot particles [14]. Statistical modeling methods have been developed based on either splitting of a large sample and measurement of several sub-samples on a gamma spectrometer [15] [35], or repetitive mixing and measuring of the same sample [36] [37] [38]. By analyzing the variance and modeling, some information about the fraction of activity in hot particles, their number, and size distribution could be inferred.

It follows from this introduction that a single gamma spectrometric measurement of a voluminous sample containing hot particles can be biased, *i.e.*, the measured activity in the sample can significantly differ from true activity. By using techniques of sample splitting or mixing followed by repetitive measurements, that bias can be reduced, however, the resulting dispersion can be large.

In environmental health risk assessment, it is most important to obtain as accurate and precise determination of activity as possible. Therefore, the aim of this investigation was to reduce bias and improve precision, when measuring voluminous samples containing hot particles. We are seeking a novel gamma Ge detector calibration model in a functional form of  $p = f(q)$ , where detector peak efficiency  $p$  is a function of empirical parameter  $q$ . In this model, we are aiming at finding  $p$  which better represents sample inhomogeneity than the bulk efficiency  $p_b$ , thereby reducing the bias and dispersion of measurement.

The methodology in this paper is by MC simulation, following [39] [40], and is described in detail in Section 2. This study focuses on a single radionuclide  $^{137}\text{Cs}$ , which is the most prominent gamma emitter remaining several years after the nuclear accident [36]. We use both the gamma radiation detected as a peak at 661.66 keV as well as Compton-scattered radiation. Scattered radiation has been used extensively in measuring void fraction using gamma radiation [41] [42] [43], medical image reconstruction [44], and geometrical inhomogeneity

[5].

In gamma spectrometry, the most significant measures of Ge detector performance are peak efficiency  $p$  as well as the total efficiency  $t$ , the latter being a sum of peak and Compton radiations [45]. The ratio of peak efficiency to total efficiency  $p/t$  is larger for larger Ge crystals and for those with Compton-suppression systems. This ratio is used in analytical approaches to coincidence-summing corrections [46]. Some authors prefer using its inverse,  $t/p$  [47]. The  $p/t$  ratio is a directly measurable quantity, at least for a single radionuclide source, and it is a strong function of gamma energy. It has been demonstrated that  $p/t$  also depends on the radioactive source position with respect to the Ge detector [48], the feature we explore in the present work.

We design two calibration models: a 1-particle model and an  $n$ -particle model. For the 1-particle model, the relation of  $p = f(p/t)$  is derived using gamma attenuation [49], and its dependence on calibration is described in Section 3. The  $n$ -particle model is described in Section 4. The effect of  $p$  vs.  $p/t$  is more complicated for this model and has to be interpolated between those for single particles and bulk sample efficiency. We describe the interpolation process using Signal Detection Theory (SDT) [50] in Section 4. The performance of the  $n$ -particle model, when activities of the particles are not equal, and the extension of the model to multi-peak radionuclide are described in Section 5, followed by discussion in Section 6 and conclusions in Section 7. In this work, we are not considering radiation counting statistics and focus exclusively on the dispersion caused by inhomogeneity.

## 2. Monte Carlo Simulations

All calculations were performed for the 661.66-keV gamma ray from  $^{137}\text{Cs}$ , using sand as sample matrix with measured density of  $1.55 \text{ g}\cdot\text{cm}^{-3}$ . Two counting geometries were considered as depicted in **Figure 1**: 0.6-L and 1-L cylindrical containers. Two coaxial p-type Ge detectors were used, with efficiencies of 134% and 48% relative to a 7.6-cm (3-inch) by 7.6-cm sodium iodide detector, which are also depicted in **Figure 1**. The dimensions in **Figure 1** are to scale, whereas the actual values are given in **Table 1**. These configurations are existing in our laboratory. They can be compared in terms of detectability, which is defined as a ratio of the sample volume to the Ge crystal volume for the same activity in both samples. The configuration 0.6 L/134% Ge has such detectability 4.8 times better than the 1 L/48% Ge configuration. However, when the samples are assumed as having the same specific activity, the detectability is the product of sample volume and the Ge crystal volume. Then, such detectability is respectively 1.7 times better.

The calculations were performed using the MC code Gespecor, version 4.2 [39]. This program is especially designed for calculations in gamma spectrometry. It tracks every gamma ray randomly emitted at randomly selected location in the sample matrix. Gamma attenuation in terms of absorption and scattering is included in the sample matrix of a given geometrical shape, as well as attenua-

tion in the Ge detector endcap and Ge crystal dead layer. Finally, gamma absorption in the Ge crystal leads to events recorded in the gamma peak, quantified as peak efficiency of the detector. Gamma scattering with partial escape from the Ge crystal leads to events outside of gamma peak in the gamma spectrum, contributing to the total efficiency of the detector. Also, gamma scattering from the lead shielding (not shown in **Figure 1**) is included. The Gespecor program accepts as input all materials elemental composition, dimensions, and densities. We performed simulations with  $10^6$  gamma-emission events in each studied case. Therefore, the calculations are realistic representations of the laboratory measurement systems. The density corrections are built into the calculations, whereas the coincidence-summing corrections [46] [48] can be included but are negligible for  $^{137}\text{Cs}$ .

In the initial step, we calculated peak and total efficiencies assuming homogeneous samples, referred to as bulk efficiencies, or Bulk efficiency model. They

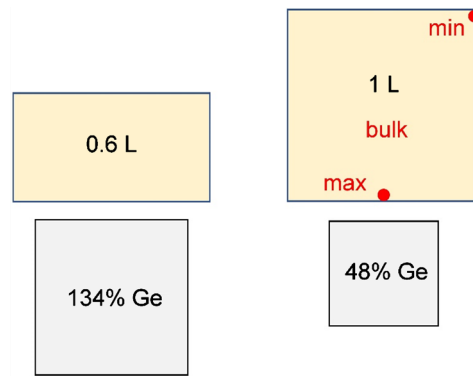


**Figure 1.** Two counting geometries which are subjects of Monte Carlo simulations: 0.6-L and 1-L cylindrical containers, and 134% and 48% Ge detectors. The relative dimensions are to scale. The actual dimensions are given in **Table 1**.

**Table 1.** Dimensions of containers and Ge crystals. Peak and total efficiencies for bulk sample as well as max, min, and average positions of hot particle.

Sample container	Ge crystal		Source position	Detection efficiency			Ratio max/min	Deviation of average from bulk (%)
	Radius (cm)	Radius (cm)		Peak	Total	<i>p/t</i>		
Height (cm)	Height (cm)	Relative efficiency (%)						
5.45	3.10		max	5.614E-02	1.931E-01	2.907E-01	73.6	-0.44
10.72	5.95		min	7.623E-04	5.501E-03	1.386E-01	35.1	-0.45
1.0	48		bulk	6.607E-03	3.372E-02	1.959E-01	2.1	0.01
			average	6.578E-03	3.357E-02	1.960E-01		
5.56	4.33		max	9.870E-02	2.731E-01	3.613E-01	18.5	-1.02
6.19	8.80		min	5.334E-03	2.404E-02	2.219E-01	11.4	-1.13
0.6	134		bulk	2.185E-02	8.221E-02	2.658E-01	1.6	0.11
			average	2.163E-02	8.129E-02	2.661E-01		

are given in **Table 1**. We also calculated efficiencies for hypothetical hot particles positioned at the closest and farthest locations, designated as max and min in **Figure 1**, respectively. It is seen that the bulk efficiency values are between those for the min and max positions. The ratio of peak efficiencies for the max and min positions is 73.6 for 1 L and 18.5 for 0.6 L. This can create significant bias in determination of hot-particle activity.

Let us abbreviate counting rate in the peak as  $R$ . The “true” activity determined using particle peak efficiency  $p$  is equal to  $A = R/p$ . The activity determined using bulk peak efficiency  $p_b$  is equal to  $A_b = R/p_b$ . The Bias is defined as

$$\text{Bias}(\%) = 100(A_b/A - 1) = 100(p/p_b - 1). \quad (1)$$

It is seen that the Bias does not depend on the activity, only on the efficiencies. Therefore, this investigation focuses on the efficiencies only. The discussion about hot particles having different activities is deferred to Section 5.

To study the effects associated with hot particles, we calculated the peak and total efficiencies of 2048 individual particles randomly distributed in either 0.6-L or 1-L containers, one particle at a time. The random positions of particles were calculated first using the algorithm for cylindrical coordinates [40]. In this algorithm, the height of particle position is proportional to a random number, while the radius of particle position is proportional to the square root of a random number. The azimuth angle is not important in this case because of a cylindrical symmetry. Then, the 2048 random particle positions were supplied to the Gespecor program, which calculated peak and total efficiencies at these positions. To verify the randomness of particle positions, we hypothesize that the average efficiency for all particles should approximate that of the bulk efficiency calculated above. The average peak and total efficiencies for all 2048 particles are also listed in **Table 1**. The deviations of average efficiencies from the bulk efficiencies are about  $-0.5\%$  for 1-L container and about  $-1\%$  for 0.6-L container, whereas the deviations for the  $p/t$  ratios are substantially smaller. The randomness of particle positions is judged satisfactory for the purpose of this study.

The biases were calculated using Eq. 1 for the 2048 particles and are plotted as histogram in **Figure 2** for 1-L container. They range from about  $-100\%$  to  $700\%$ , or by a factor of 8. This is less than 73.6 listed in **Table 1**, however, it is statistically unlikely to have a particle located at either a min or a max position. The frequency distribution of the biases is depicted in **Figure 3** (distribution a, green points). This distribution resembles an exponential, reflecting exponential attenuation of gamma radiation in the sample.

### 3. One-Particle Model

The 1-particle model assumes presence of a single hot particle in the sample. This model provides a foundation for the  $n$ -particle model to be described in the next section. Let us consider a particle in the sample matrix located at a distance  $r$  from the Ge detector. In a simplified picture, we neglect all possible angles and

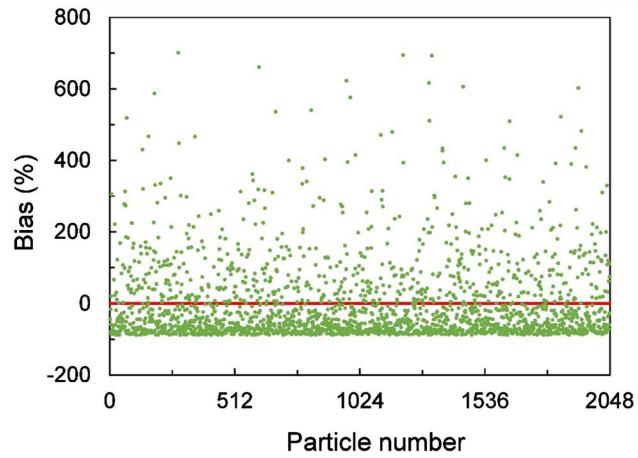


**Figure 2.** Histogram of Bias from single particle efficiency when using bulk efficiency for 1-L container.

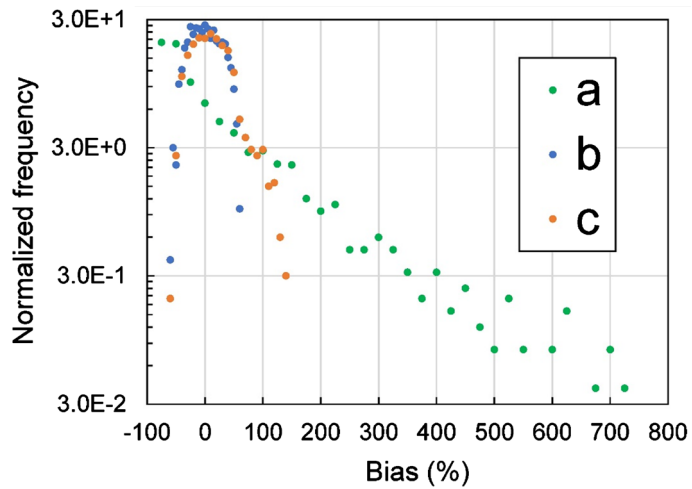


**Figure 3.** Frequency plots for various Bias distributions for 1-L container. (a) Bias bulk from single particle, bin size 25%; (b) Bias for 1-particle model, bin size 5%; (c) Bias for  $n$ -particle model applied to 1 particle, bin size 10%.

finite sizes of both sample and the detector. For a gamma photon to be detected in the peak with efficiency  $p_r$ , it must be attenuated in the sample and detected with an intrinsic peak efficiency of the detector  $p_d$ . We thus have

$$p_r = p_d \exp(-\mu_0 r). \tag{2}$$

Similar considerations apply to the total efficiency  $t_r$  and intrinsic detector  $t_d$ . However, the total efficiency is enhanced by the scattered radiation in the sample originating from gamma photons emitted at the particle location  $r$ . Therefore,

$$t_r = t_d \exp(-\mu_0 r) \exp(\mu_s r). \tag{3}$$

Also,

$$\mu_0 = \mu_a + \mu_s + \text{minor terms}, \tag{4}$$

where  $\mu_0$  is a total gamma attenuation coefficient,  $\mu_a$  is a gamma absorption

coefficient, and  $\mu_s$  is an incoherent (Compton) scattering coefficient [49].

By manipulation of Equations (2) and (3), we obtain

$$\frac{p_r}{p_d} = \left( \frac{t_d p_r}{p_d t_r} \right)^{\mu_0/\mu_s}. \quad (5)$$

It follows that  $p$  should be a power function of  $p/t$ ,

$$p = g (p/t)^h, \quad (6)$$

where  $g$  and  $h$  are coefficients. In this way  $p/t$  carries some information about hot-particle peak efficiency and thus its position.

The  $p$  values are plotted as a function of  $p/t$  for the 1-L container in **Figure 4**. The densely located 2048 points lump into a gray area. The reason for such wide distribution is that it involves random particle locations and all directions of gamma emissions from a particle, as well as taking the ratio of two random variables  $p/t$ . Then an unconstrained power-law fit was made to the points according to Equation (6) resulting in  $p_u$ , depicted by the green curve in **Figure 4** representing the most probable  $p$ .

The sequence of analyzing the data is as follows. For each simulated particle at its location, one calculates  $p/t$  obtained from the MC simulation. Experimentally, for a single radionuclide, it would correspond to taking a ratio of the counts in the peak to the total counts in the gamma spectrum. Then, one reads the most probable value  $p_u$  from the green curve in **Figure 4**. Subsequently, one calculates the Bias from Equation (1), by substituting  $p_u$  for  $p_b$ .

The histogram of Bias values for 1-particle model is depicted in **Figure 5**. It is seen that bias now spans the range between about  $-60\%$  and  $60\%$ , and it is significantly reduced from that for the bulk efficiency in **Figure 2**. The frequency distribution for 1-particle model is depicted as curve b in **Figure 3** (blue points).

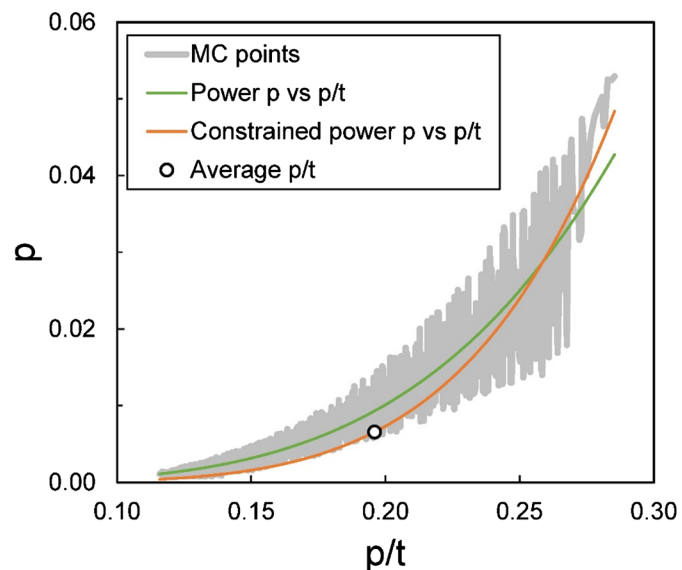


**Figure 4.** Plots of  $p$  as a function of  $p/t$  for the MC data and various fits described in the text.

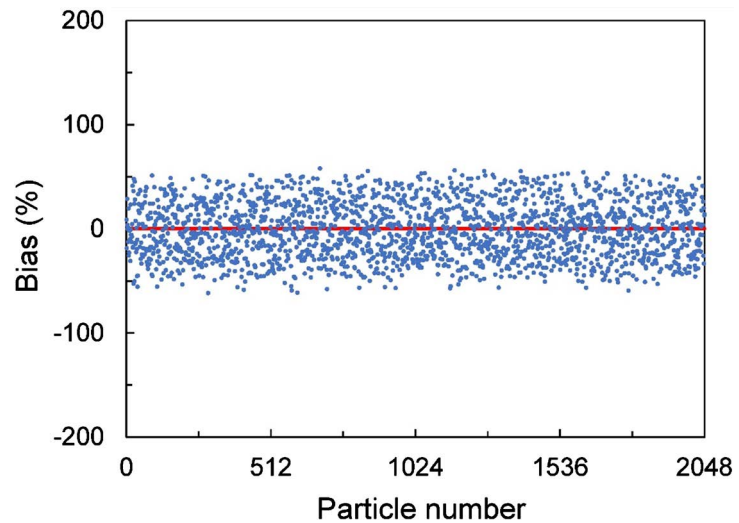


**Figure 5.** Histogram of Bias from single particle efficiency when using 1-particle model efficiency for 1-L container.

It is a narrow symmetric distribution reflecting significant reduction in the dispersion of the results.

#### 4. $n$ -Particle Model

The  $n$ -particle model assumes that there are 1 or more hot particles in the sample, all having the same activity. It can be realized by simple grouping of the 2048 MC points. For instance, one can group 2 particles (1024 cases), 4 particles (512 cases), etc., until finally arriving at 1 case of 2048 particles. The average variables for  $n$  independent particles are given by

$$\langle p \rangle_n = \frac{1}{n} \sum_{i=1}^n p_i, \quad (7)$$

$$\langle t \rangle_n = \frac{1}{n} \sum_{i=1}^n t_i, \quad (8)$$

$$\langle p/t \rangle_n = \langle p \rangle_n / \langle t \rangle_n, \quad (9)$$

The reason for such definitions of averages is that Equation (9) is the one that would be realized experimentally. The averages are “true” values as calculated by the MC program, and the Bias when using Bulk efficiency model is generalized from Equation (1):

$$\text{Bias}(\%) = 100 \left( \langle p \rangle_n / p_b - 1 \right). \quad (10)$$

The values of  $\langle p \rangle_{2048}$ ,  $\langle t \rangle_{2048}$ , and  $\langle p/t \rangle_{2048}$  are listed in **Table 1** under source position in the average row (both geometries). As discussed in Section 2, the averages for 2048 particles approximate bulk efficiency calculations  $p_b$ ,  $t_b$ , and  $(p/t)_b$  very well. This average for 1 L container is depicted as an open circle in **Figure 4**, which does not lay on the green  $p_u$  curve. The reason is that  $\langle p/t \rangle_n$  (Equation (9)) is not equal to  $1/n \sum_{i=1}^n p_i / t_i$ .

We performed another power-law fit to the data in **Figure 4**, this time we

constrained the fit by passing through the  $\langle p/t \rangle_{2048}$  point, resulting in an orange  $p_c$  curve. It follows that, regardless of the number of hot particles present, the most probable measured  $p/t$  will fall between these two curves. Therefore, we need to interpolate between them in such a way that if  $p/t$  is close to  $\langle p/t \rangle_{2048}$ , it will be weighted towards  $p_s$ ; if it is far from  $\langle p/t \rangle_{2048}$ , then it will be weighted towards  $p_u$ . We tried linear and quadratic interpolations without success because the interpolation has to be steep in the vicinity of  $\langle p/t \rangle_{2048}$ .

A satisfactory interpolation can be obtained however, by application of the SDT [50]. SDT is concerned with distinguishing between the signal and noise. We assume Gaussian distributions for both signal and noise, with the mean and sigma given as  $\{\mu_{\text{signal}}, \sigma_{\text{signal}}\}$  and  $\{\mu_{\text{noise}}, \sigma_{\text{noise}}\}$ , respectively. We designate a Gaussian (normal) distribution function (an integral of the Gaussian probability density function from minus infinity to the Deviate) with mean and sigma, and its inverse as

$$\text{Probability} = \Phi(\text{Deviate}, \{\text{mean}, \text{sigma}\}), \quad (11)$$

$$\text{Deviate} = \Phi^{-1}(\text{Probability}, \{\text{mean}, \text{sigma}\}). \quad (12)$$

For the set of 2048 points, we find the minimum and maximum values of  $p/t$ ,  $(p/t)_{\min}$  and  $(p/t)_{\max}$ , respectively. For any average of  $n$  particles, the SDT probability of signal rejection,  $P_r$  can be written as

$$P_r = \begin{cases} \frac{\langle p/t \rangle_n - (p/t)_{\min}}{\langle p/t \rangle_{2048} - (p/t)_{\min}}, & \langle p/t \rangle_n \leq \langle p/t \rangle_{2048}, \\ \frac{(p/t)_{\max} - \langle p/t \rangle_n}{(p/t)_{\max} - \langle p/t \rangle_{2048}}, & \langle p/t \rangle_n > \langle p/t \rangle_{2048}. \end{cases} \quad (13a)$$

$$P_r = \begin{cases} \frac{\langle p/t \rangle_n - (p/t)_{\min}}{\langle p/t \rangle_{2048} - (p/t)_{\min}}, & \langle p/t \rangle_n \leq \langle p/t \rangle_{2048}, \\ \frac{(p/t)_{\max} - \langle p/t \rangle_n}{(p/t)_{\max} - \langle p/t \rangle_{2048}}, & \langle p/t \rangle_n > \langle p/t \rangle_{2048}. \end{cases} \quad (13b)$$

Then, by combining Equations (11)-(13), we obtain the SDT probability of misses  $P_m$  and hits  $P_h$  as

$$P_m = \Phi\left[\Phi^{-1}(P_r, \{\mu_{\text{noise}}, \sigma_{\text{noise}}\}), \{\mu_{\text{signal}}, \sigma_{\text{signal}}\}\right], \quad (14a)$$

$$P_h = 1 - P_m. \quad (14b)$$

We determined that a mean and sigma of  $\{0, 1\}$  for the noise, and  $\{0.6, 0.5\}$  for the signal, provided sufficient convergence.

Finally, the interpolated value of  $p_{\text{interp}}$  between the unconstrained fit  $p_u$  and the constrained fit  $p_c$  from **Figure 4** (green and orange curves, respectively) is given by

$$p_{\text{interp}} = P_h p_u + P_m p_c. \quad (15)$$

The Bias for the  $n$ -particle model is given by

$$\text{Bias}(\%) = 100\left(\langle p \rangle_n / p_{\text{interp}} - 1\right). \quad (16)$$

The performance of various models is listed in **Table 2** for 1-L container. The quantity of interest is the Bias(%) from “true” efficiencies known from the MC calculation, its minimum (Min) and maximum (Max) values, as well as standard deviation (Std Dev). **Table 2** shows that for 1 particle, the Bulk efficiency model

resulted in a significant minimum and maximum bias and bias standard deviation. This was already seen in **Figure 1** and **Figure 2**. As the number of particles increases, the bias and all its measures decrease since the inhomogeneity drops. Application of 1-particle model to 1 particle present significantly reduces the bias and its standard deviation. Application of  $n$ -particle model reduces all measures of bias as compared with the Bulk model, for all particles studied. The  $n$ -particle model applied to 1 particle performs slightly worse than the 1-particle model. This is seen in the bias measures in **Table 2**, as well as in the frequency distribution with right tail (curve c in **Figure 3**).

The results of the Bias for the 0.6-L container are listed in **Table 3**. They exhibit the same trends as for the 1-L container, however, of smaller magnitude

**Table 2.** Performance of the Bulk,  $n$ -particle, and 1-particle models expressed as bias from known efficiency for several number of particles and 1-L container.

Model	Number of particles	Bias (%)						
		1	2	4	8	16	32	64
Bulk	Min	-88.1	-86.2	-79.1	-76.2	-54.9	-48.2	-29.6
	Max	701.2	430.1	257.9	151.0	84.4	41.2	33.6
	Std Dev	114.7	79.3	58.1	41.4	29.7	20.8	14.9
$n$ -particle	Min	-61.7	-63.3	-56.9	-56.9	-35.4	-22.7	-18.9
	Max	137.5	117.1	74.0	62.5	43.3	21.2	24.4
	Std Dev	35.7	27.8	22.5	20.4	15.9	11.5	9.6
1-particle	Min	-61.7						
	Max	57.9						
	Std Dev	26.5						

**Table 3.** Performance of the Bulk,  $n$ -particle, and 1-particle models expressed as bias from known efficiency for several number of particles and 0.6-L container.

Model	Number of particles	Bias (%)						
		1	2	4	8	16	32	64
Bulk	Min	-74.7	-73.3	-66.9	-49.8	-41.6	-22.0	-13.7
	Max	326.9	223.4	157.7	97.3	55.4	27.3	14.1
	Std Dev	70.4	50.6	36.2	26.3	17.3	10.3	7.2
$n$ -particle	Min	-49.1	-45.7	-42.1	-32.9	-20.7	-12.4	-6.5
	Max	74.1	60.5	50.8	39.5	17.5	11.3	8.0
	Std Dev	25.4	19.2	14.7	11.1	7.8	6.0	3.7
1-particle	Min	-49.2						
	Max	52.6						
	Std Dev	23.2						

reflecting relatively less inhomogeneity in this smaller container.

In order to compare model performances for the two containers, we define Bias Range (%) as the difference between the Max and Min bias. Then, the improvement factors for the Bias Range and Bias Std Dev (%) are calculated as the ratios of the corresponding values from the Bulk model to the ones for the 1-particle and  $n$ -particle models. The improvement factors are depicted in **Figure 6** for 1 and more particles present in the sample. It is seen that there are significant improvements in Bias Range and Bias Std Dev when using the calibration models developed here. The highest improvements by a factor ranging from about 3 to 6.5 are when using 1-particle model. The same case of 1 particle present, when applying the  $n$ -particle model to it, resulted in improvement factors from about 3 to 4. As the number of particles increases, the improvement factors drop to between 1.5 and 2 for 64 particles. For small number of particles (1 to 4), the improvement factors are higher for 1-L container than for the 0.6-L container; this trend is reversed for larger number of particles in most cases.

## 5. Non-Equal Particles and Multi-Peak Radionuclide

The  $n$ -particle model assumes that all particles have the same activities. It was observed that hot particles from nuclear accidents exhibit distribution of sizes [14], often assumed lognormal [15]. Then, constant specific activity implies lognormal distribution of activities as well. This situation results in even more inhomogeneity than for equal particles, because a few of very hot particles dominate activity of the sample.

Non-equal particles can be easily simulated within the present data set by positioning several equal particles in the same location. Since the derived  $n$ -particle

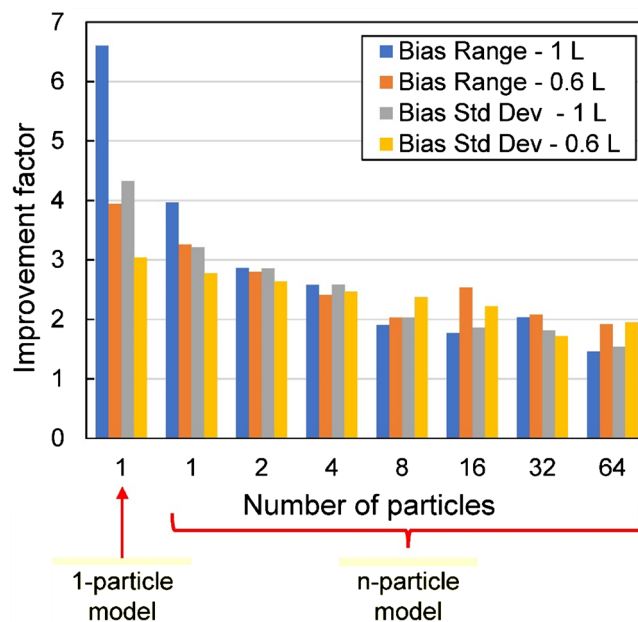


**Figure 6.** Improvement factors for Bias Range and Bias Std Dev when using 1-particle and  $n$ -particle models compared with the Bulk model, for 1-L and 0.6-L containers.

model interpolates the efficiencies between 1 particle and the bulk sample, it should be independent of a specific assumption about the number or location of the particles. Therefore, it should apply to non-equal particles as well.

To test this hypothesis, we created two cases of non-equal particles, for 1-L container. In the first case we have 2 particles, one is assumed twice as radioactive as the other. Therefore, the average peak efficiency from Equation (7) is  $\langle p \rangle_2 = 1/3(2p_1 + p_2)$ . We have used 2 equal particles from the MC set of 2048 and created a group of 2 non-equal particles. We have 1024 such groups to perform statistics on. For the second case, we repeated 1<sup>st</sup> particle 4 times, 2<sup>nd</sup> particle 2 times, and took the 3<sup>rd</sup> and 4<sup>th</sup> particles as is. The average peak efficiency is  $\langle p \rangle_4 = 1/8(4p_1 + 2p_2 + p_3 + p_4)$ . We thus have 512 such groups. Similarly, we calculated  $\langle t \rangle_n$  and  $\langle p/t \rangle_n$ ,  $n = 2, 4$ . Then, we apply the  $n$ -particle model by calculating  $p_{interp}$  from Equation (15) and study the Bias from Equation (16).

The results are given in **Table 4** in terms of Bias Range and Bias Std Dev. Also, the results for equal 1, 2, and 4 particles are reproduced from **Table 2**. It is seen that the values for 2 non-equal particles are laying between those for 1 and 2 equal particles. The reason is that one particle dominates by assumption. For the case of 4 non-equal particles, the values are between those for 2 and 4 equal particles because of assumed distribution of activity among particles and domination by the hotter ones. Nevertheless, the  $n$ -particle model performed well and the calculated values of Bias Range and Bias Std Dev are significantly improved from those of the Bulk model.

In this work we have considered a single gamma peak of 661.11 keV from  $^{137}\text{Cs}$ . The  $n$ -particle model based on  $p/t$  can be extended to multi-peak radionuclide as follows. Let  $A$  represent the radionuclide activity of a hot particle. The counting rate in gamma peak  $j$  is given by

$$R_{p,j} = Ap_{eff,j}, \quad (17)$$

where  $p_{eff,j}$  is an effective peak efficiency, which includes gamma intensity, density correction in the sample matrix and any coincidence-summing correction. For  $k$  peaks of the radionuclide in the gamma spectrum, the total counting rate in all peaks is equal to

$$R_p = \sum_{j=1}^k R_{p,j} = A \sum_{j=1}^k p_{eff,j} = Ap_{eff}. \quad (18)$$

**Table 4.** Performance of the  $n$ -particle model for non-equal particles in 1-L container.

	Number of particles		
	1	2	4
Equal particles			
Bias Range (%)	199.2	180.3	130.9
Bias Std Dev (%)	35.7	27.8	22.5
Non-equal particles		2	4
Bias Range (%)		188.0	168.0
Bias Std Dev (%)		29.6	26.0

Similarly, for the total counting rate,

$$R_t = \sum_{j=1}^k R_{t,j} = A \sum_{j=1}^k t_{eff,j} = A t_{eff}. \quad (19)$$

Therefore, the observed peak-to-total ratio for a multi-peak radionuclide is given by

$$(p/t)_{eff} = R_p / R_t = p_{eff} / t_{eff}. \quad (20)$$

The left-hand side of Equation (20) can be measured, while the right-hand side calculated by the MC simulation. The  $n$ -particle model can be used as earlier in Sections 4, 5, with  $p$  and  $t$  replaced by  $p_{eff}$  and  $t_{eff}$ .

## 6. Discussion

A overview of the origins and behavior of hot particles was provided in Section 1. Such particles are normally encountered in environmental samples following nuclear accidents. Digital radiography is typically used for samples spread on a surface, while digital tomography is not always practical for measuring many environmental samples. Surveillance samples for gamma spectrometry are typically large to increase sensitivity and to provide better sampling of radioactive contamination. However, voluminous samples may be inhomogeneous due to the presence of hot particles. Applying the Bulk efficiency model leads to significant bias of measured activity. One approach to this problem is repetitive mixing and measuring of a sample (from 25 to 100 times [36] [38]). While this method can provide relatively accurate average of the measured activity, is not very practical for many samples, and the dispersion evaluated by means of a standard deviation can be large and increasing as the number of hot particle decreases.

In this investigation we provided a method to reduce this dispersion. Our goal was to study the behavior of hot particles randomly distributed in the soil matrix, for two counting geometries: 1-L and 0.6-L cylindrical containers. Using MC simulation, we calculated the peak and total efficiencies of 2048 individual hot particles at random locations in each container. We focused on a single radionuclide of  $^{137}\text{Cs}$  and its 661.66-keV gamma ray. The presence of counts in the gamma peak in the spectrum represents gamma transmission, whereas anywhere in the gamma spectrum, both transmission and scattering. On this basis, we derived a power-law relationship between peak efficiency and peak-to-total ratio. This relationship was confirmed by the MC simulation. Since peak-to-total ratio is a measurable parameter, the power-law relationship can provide a more accurate value of the efficiency than the bulk efficiency. We called this approach 1-particle model. It was shown that the 1-particle model reduced the Bias Range 6.5 times and Bias Std Dev 4 times compared to the Bulk efficiency model for 1-L container, and 4 and 3 times for 0.6-L container, respectively.

Subsequently, identical individual particles were combined into  $n$ -particle groups, which resulted in the  $n$ -particle model. The averages for peak and total

efficiencies were calculated as well as their peak-to-total ratio. From the power-law relationship, the most probable value of peak efficiency could be obtained from the empirically available peak-to-total ratio. The complication arose from the fact that the most probable peak efficiency lays between the single-particle power-law and the power-law constrained by the bulk efficiency point. Fortunately, an innovative interpolation was developed, based on a formulation from the Signal Detection Theory, between the two power-law curves. The  $n$ -particle model works well for any number of particles. When applied to a single-particle case, the reduction in Bias Range and Bias Std Dev was between 3 and 4. These are improvement factors when using this model compared with the Bulk model. As the number of hot particles increases, the inhomogeneity decreases, and improvement factors decrease to between 1.5 and 2 for 64 hot particles. We also simulated groups of non-equal hot particles and found that the  $n$ -particle model is independent of the number, location, and size distribution of hot particles.

If this approach is applied to repetitive mixing and measurement method for inhomogeneous sample, the accuracy of the average is expected to have low bias as before, however, the standard deviation will decrease several times. If only one measurement is made on an unknown sample, this method guarantees reduction of the bias several times for inhomogeneous samples without the need of knowing the details of inhomogeneity.

## 7. Conclusion

We developed a novel calibration of a gamma-ray spectrometer using the relationship  $p = g(p/t)^h$ , where  $g$  and  $h$  are coefficients and  $p/t$  is a ratio of peak-to-total efficiencies. This method can be used to reduce the variance of measured activity in bulk environmental or food samples containing hot particles as compared with the homogenous calibration. So far, we were able to apply it to a single-peak single-radionuclide, such as  $^{137}\text{Cs}$ , which is known as the most important gamma emitter for aged fallout from nuclear-power accidents. We also derived equations to accommodate multiple-peak radionuclide. At this time, the method has not been shown suitable for characterizing samples containing mixtures of radionuclides.

## Acknowledgements

This work was partially supported by the US FDA FERN Cooperative Agreement 1U18FD005514.

## Conflicts of Interest

The authors declare no conflicts of interest regarding the publication of this paper.

## References

- [1] Biagini, R., Dersch, R., de Felice, P., Jerome, S.M., Perkin, E.M.E., Pona, C., de Sa-

- noit, J. and Woods, M.J. (1995) Homogeneity Testing of Spiked Reference Materials. *Science of the Total Environment*, **173-174**, 267-274.  
[https://doi.org/10.1016/0048-9697\(95\)04751-4](https://doi.org/10.1016/0048-9697(95)04751-4)
- [2] Korun, M., Martinčič, R. and Merkan, M. (1996) Determination of the Activities in Inhomogeneous Samples by Gamma Spectrometry Using Energy-Dependent Self-Absorption. *Nuclear Instruments and Methods in Physics Research Section A*, **369**, 681-683. [https://doi.org/10.1016/S0168-9002\(96\)80075-1](https://doi.org/10.1016/S0168-9002(96)80075-1)
- [3] Gharbi, F. (2011) Inhomogeneity Effects on HPGe Gamma Spectrometry Detection Efficiency Using Monte Carlo Technique. *Nuclear Instruments and Methods in Physics Research Section A*, **654**, 266-271.  
<https://doi.org/10.1016/j.nima.2011.06.055>
- [4] IEEE (The Institute of Electrical and Electronics Engineers) (1978) ANSI/IEEE Standard 680-1978: IEEE Standard Techniques for Determination of Germanium Semiconductor Detector Gamma-Ray Efficiency Using a Standard Marinelli (Reentrant) Beaker Geometry. The Institute of Electrical and Electronics Engineers, New York. <https://doi.org/10.1109/IEEESTD.1978.7434538>
- [5] Zamzamian, S.M., Hosseini, S.A., Fegghi, S.A. and Samadfam, M. (2020) Determining of the Optimized Dimensions of the Marinelli Beaker Containing Source with Inhomogeneous Emission Rate by Using Genetic Algorithm Coupled with MCNP and Determining Distribution Type by Neural Networks. *Applied Radiation and Isotopes*, **157**, Article No. 109039.  
<https://doi.org/10.1016/j.apradiso.2020.109039>
- [6] Bronson, F. (2010) How Well Does a Gamma Spectroscopy Calibration with a Uniform Density Matrix Represent a Sample with a Non-Uniform Matrix? *56th Annual Radiobioassay and Radiochemical Measurements Conference*, Richland, 25-28 October 2010.
- [7] Semkow, T.M., Bradt, C.J., Beach, S.E., Haines, D.K., Khan, A.J., Bari, A., Torres, M.A., Marrantino, J.C., Syed, U.-F., Kitto, M.E., Hoffman, T.J. and Curtis, P. (2015) Calibration of Ge Gamma-Ray Spectrometers for Complex Sample Geometries and Matrices. *Nuclear Instruments and Methods in Physics Research Section A*, **799**, 105-113. <https://doi.org/10.1016/j.nima.2015.07.064>
- [8] Adams, C.E., Farlow, N.H. and Schell, W.R. (1960) The Compositions, Structures and Origin of Radioactive Fall-Out Particles. *Geochimica et Cosmochimica Acta*, **18**, 42-56. [https://doi.org/10.1016/0016-7037\(60\)90016-8](https://doi.org/10.1016/0016-7037(60)90016-8)
- [9] Sandalls, F.J., Segal, M.G. and Victorova, N. (1993) Hot Particles from Chernobyl: A Review. *Journal of Environmental Radioactivity*, **18**, 5-22.  
[https://doi.org/10.1016/0265-931X\(93\)90063-D](https://doi.org/10.1016/0265-931X(93)90063-D)
- [10] Zheltonozhsky, V., Mück, K. and Bondarkov, M. (2001) Classification of Hot Particles from the Chernobyl Accident and Nuclear Weapons Detonations by Non-Destructive Methods *Journal of Environmental Radioactivity*, **57**, 151-166.  
[https://doi.org/10.1016/S0265-931X\(01\)00013-3](https://doi.org/10.1016/S0265-931X(01)00013-3)
- [11] Igarashi, Y., Kogure, T., Kurihara, Y., Miura, H., Okumura, T., Satouf, Y., Takahashic, Y. and Yamaguchi, N. (2019) A Review of Cs-Bearing Microparticles in the Environment Emitted by the Fukushima Dai-ichi Nuclear Power Plant Accident. *Journal of Environmental Radioactivity*, **205-206**, 101-118.  
<https://doi.org/10.1016/j.jenvrad.2019.04.011>
- [12] Futagami, F., Soliman, M., Takamiya, K., Sekimoto, S., Oki, Y., Kubota, T., Konno, M., Mizuno, S. and Ohtsuki, T. (2020) Isolation, Characterization and Source Analysis of Radiocaesium Micro-Particles in Soil Sample Collected from Vicinity of Fukushima Dai-ichi Nuclear Power Plant. *Journal of Environmental Radioactivity*,

- 223-224**, Article ID: 106388. <https://doi.org/10.1016/j.jenvrad.2020.106388>
- [13] Ansoborlo, E. and Stather, J. (2000) Review of the Characterization of Hot Particles Released into the Environment and Pathways for Intake of Particles. *Radiation Protection Dosimetry*, **92**, 139-143. <https://doi.org/10.1093/oxfordjournals.rpd.a033259>
- [14] Tcherkezian, V., Shkinev, V., Khitrov, L. and Kolesov, G. (1994) Experimental Approach to Chernobyl Hot Particles. *Journal of Environmental Radioactivity*, **22**, 127-139. [https://doi.org/10.1016/0265-931X\(94\)90018-3](https://doi.org/10.1016/0265-931X(94)90018-3)
- [15] Shevchenko, S.V. (2004) On the Uncertainty in Activity Measurements for Samples containing “Hot Particles”. *Applied Radiation and Isotopes*, **61**, 1303-1306. <https://doi.org/10.1016/j.apradiso.2004.02.022>
- [16] Tian, Z., Ouyang, X., Liu, L., Ruan, J. and Liu, J. (2015) A Theoretical and Experimental Research on Detection Efficiency of HPGe Detector for Disc Source with Heterogeneous Distribution. *Journal of Radioanalytical and Nuclear Chemistry*, **304**, 905-910. <https://doi.org/10.1007/s10967-014-3907-2>
- [17] Masson, O., Baeza, A., Bieringer, J., Brudecki, K., Bucci, S., Cappai, M., *et al.* (2011) Tracking of Airborne Radionuclides from the Damaged Fukushima Dai-Ichi Nuclear Reactors by European Networks. *Environmental Science & Technology*, **45**, 7670-7677. <https://doi.org/10.1021/es2017158>
- [18] Kaltofen, M. and Gundersen, A. (2017) Radioactively-Hot Particles Detected in Dusts and Soils from Northern Japan by Combination of Gamma Spectrometry, Autoradiography, and SEM/EDS Analysis and Implications in Radiation Risk Assessment. *Science of the Total Environment*, **607-608**, 1065-1072. <https://doi.org/10.1016/j.scitotenv.2017.07.091>
- [19] Kitto, M.E., Menia, T.A., Haines, D.K., Beach, S.E., Bradt, C.J., Fielman, E.M., Syed, U.-F., Semkow, T.M., Bari, A. and Khan, A.J. (2013) Airborne Gamma-Ray Emitters from Fukushima Detected in New York State. *Journal of Radioanalytical and Nuclear Chemistry*, **296**, 49-56. <https://doi.org/10.1007/s10967-012-2043-0>
- [20] Bondarkov, M.D., Zheltonozhsky, V.A., Zheltonozhskaya, M.V., Kulich, N.V., Maksimenko, A.M., Farfán, E.B., Jannik, G.T. and Marra, J.C. (2011) Assessment of the Radionuclide Composition of “Hot Particles” Sampled in the Chernobyl Nuclear Power Plant Fourth Reactor Unit. *Health Physics*, **101**, 368-374. <https://doi.org/10.1097/HP.0b013e31820dbc53>
- [21] Nageldinger, G., Flowers, A. and Entwistle, J. (1998) A New Mechanism for Hot Particle Development in Soil Following Ionic Contamination with Radiocesium. *Health Physics*, **75**, 646-647. <https://doi.org/10.1097/00004032-199812000-00009>
- [22] Charles, M.W. (1991) The Hot Particle Problem. *Radiation Protection Dosimetry*, **39**, 39-47.
- [23] Byrnes, I., Lind, O.C., Hansen, E.L., Janssens, K. and Salbu, B. (2020) Characterization of Radioactive Particles from the Dounreay Nuclear Reprocessing Facility. *Science of the Total Environment*, **727**, Article ID: 138488. <https://doi.org/10.1016/j.scitotenv.2020.138488>
- [24] EPA (Environmental Protection Agency) (2009) Radiological Laboratory Sample Analysis Guide for Incidents of National Significance—Radionuclides in Air. US Environmental Protection Agency, Report EPA 402-R-09-007, National Air and Radiation Environmental Laboratory, Montgomery, AL.
- [25] Zeissler, C.J., Lindstrom, R.M. and McKinley, J.P. (2001) Radioactive Particle Analysis by Digital Radiography. *Journal of Radioanalytical and Nuclear Chemistry*, **248**, 407-412. <https://doi.org/10.1023/A:1010640411441>

- [26] Dung, T.Q. (1998) Some Theoretical Results of Gamma Techniques for Measuring large Samples. *Nuclear Instruments and Methods in Physics Research Section A*, **416**, 505-515. [https://doi.org/10.1016/S0168-9002\(98\)00622-6](https://doi.org/10.1016/S0168-9002(98)00622-6)
- [27] Krings, T. and Mauerhofer, E. (2011) Reconstruction of the Activity of Point Sources for the Accurate Characterization of Nuclear Waste Drums by Segmented Gamma Scanning. *Applied Radiation and Isotopes*, **69**, 880-889. <https://doi.org/10.1016/j.apradiso.2011.02.009>
- [28] Stanga, D. and Gurau, D. (2012) A New Approach in Gamma-Rays Canning of Rotating Drums Containing Radioactive Waste. *Applied Radiation and Isotopes*, **70**, 2149-2153. <https://doi.org/10.1016/j.apradiso.2012.02.085>
- [29] Wang, K., Li, Z. and Feng, W. (2014) Reconstruction of Finer Voxel Grid Transmission Images in Tomographic Gamma Scanning. *Nuclear Instruments and Methods in Physics Research Section A*, **755**, 28-31. <https://doi.org/10.1016/j.nima.2014.04.046>
- [30] Glavič-Cindro, D., Korun, M., Vodenik, B. and Zorko, B. (2015) Activity Measurements of Barrels Filled with Radioactive Waste. *Journal of Radioanalytical and Nuclear Chemistry*, **304**, 145-150. <https://doi.org/10.1007/s10967-014-3666-0>
- [31] Maxwell, S.L., Culligan, B.K., Kelsey-Wall, A. and Shaw, P.J. (2012) Rapid Determination of Actinides in Emergency Food Samples. *Journal of Radioanalytical and Nuclear Chemistry*, **292**, 339-347. <https://doi.org/10.1007/s10967-011-1411-5>
- [32] Parekh, P.P., Semkow, T.M., Torres, M.A., Haines, D.K., Cooper, J.M., Rosenberg, P.M. and Kitto, M.E. (2006) Radioactivity in Trinitite Six Decades Later. *Journal of Environmental Radioactivity*, **85**, 103-120. <https://doi.org/10.1016/j.jenvrad.2005.01.017>
- [33] Nishikawa, K., Bari, A., Khan, A.J., Li, X., Menia, T., Semkow, T.M., Lin, Z. and Healey, S. (2017) Homogenization of Food Samples for Gamma Spectrometry Using Tetramethylammonium Hydroxide and Enzymatic Digestion. *Journal of Radioanalytical and Nuclear Chemistry*, **314**, 859-870. <https://doi.org/10.1007/s10967-017-5434-4>
- [34] Nishikawa, K., Bari, A., Khan, A.J., Li, X., Menia, T. and Semkow, T.M. (2018) Homogenization of Food Samples for Gamma Spectrometry Using Protease. *Journal of Radioanalytical and Nuclear Chemistry*, **318**, 401-406. <https://doi.org/10.1007/s10967-018-6065-0>
- [35] Bunzl, K. (1997) Probability for Detecting Hot Particles in Environmental Samples by Sample Splitting. *The Analyst*, **122**, 653-656. <https://doi.org/10.1039/A700252A>
- [36] Nageldinger, G., Flowers, A., Henry, B. and Postak, J. (1998) Hot Particle Detection Using Uncertainties in Activity Measurements of Soil. *Health Physics*, **74**, 472-477. <https://doi.org/10.1097/00004032-199804000-00009>
- [37] Bunzl, K. (1998) Detection of the Radioactive Hot Particles in Environmental Samples by Repeated Mixing. *Applied Radiation and Isotopes*, **49**, 1625-1631. [https://doi.org/10.1016/S0969-8043\(98\)00002-5](https://doi.org/10.1016/S0969-8043(98)00002-5)
- [38] Kashparov, V.A., Yoshchenko, V.I., Levchuk, S.E., Tschiersch, J. and Wagenpfeil, F. (2000) Application of the Method of Repeated Mixing to Nonuniformity Contaminated Bulky Samples. *Journal of Radioanalytical and Nuclear Chemistry*, **246**, 165-172. <https://doi.org/10.1023/A:1006738727056>
- [39] Sima, O., Arnold, D. and Dovlete, C. (2001) GESPECOR: A Versatile Tool in Gamma-Ray Spectrometry. *Journal of Radioanalytical and Nuclear Chemistry*, **248**, 359-364. <https://doi.org/10.1023/A:1010619806898>
- [40] Sima, O. (2012) Efficiency Calculation of Gamma Detectors by Monte Carlo Me-

- thods. In: *Encyclopedia of Analytical Chemistry, Nuclear Methods*, J. Wiley & Sons, New York, 1-37. <https://doi.org/10.1002/9780470027318.a9142>
- [41] Åbro, E., Khoryakov, V.A., Johansen, G.A. and Kocbach, L. (1999) Determination of Void Fraction and Flow Regime Using a Neural Network Trained on Simulated Data Based on Gamma-Ray Densitometry. *Measurement Science and Technology*, **10**, 619-630. <https://doi.org/10.1088/0957-0233/10/7/308>
- [42] El Abd, A. (2014) Intercomparison of Gamma Ray Scattering and Transmission Techniques for Gas Volume Fraction Measurements in Two Phase Pipe Flow. *Nuclear Instruments and Methods in Physics Research Section A*, **735**, 260-266. <https://doi.org/10.1016/j.nima.2013.09.047>
- [43] Roshani, G.H., Nazemi, E. and Feghhi, S.A.H. (2016) Investigation of Using  $^{60}\text{Co}$  Source and One Detector for Determining the Flow Regime and Void Fraction in Gas-Liquid Two-Phase Flows. *Flow Measurement and Instrumentation*, **50**, 73-79. <https://doi.org/10.1016/j.flowmeasinst.2016.06.013>
- [44] Frandes, M., Timar, B. and Lungeanu, D. (2016) Image Reconstruction Techniques for Compton Scattering Based Imaging: An Overview. *Current Medical Imaging Reviews*, **12**, 95-105. <https://doi.org/10.2174/1573405612666160128233916>
- [45] Korun, M. (2004) Measurement of Peak and Total Efficiencies of Low-Energy Gamma-Ray Detectors with Sources Emitting Photons in Cascade. *Applied Radiation and Isotopes*, **60**, 207-211. <https://doi.org/10.1016/j.apradiso.2003.11.018>
- [46] Semkow, T.M., Mehmood, G., Parekh, P.P. and Virgil, M. (1990) Coincidence Summing in Gamma-Ray Spectroscopy. *Nuclear Instruments and Methods in Physics Research Section A*, **290**, 437-444. [https://doi.org/10.1016/0168-9002\(90\)90561-J](https://doi.org/10.1016/0168-9002(90)90561-J)
- [47] Korun, M. (2001) Measurement of the Total-to-Peak Ratio of a Low-Energy Germanium Gamma-Ray Detector. *Nuclear Instruments and Methods in Physics Research Section A*, **457**, 245-252. [https://doi.org/10.1016/S0168-9002\(00\)00745-2](https://doi.org/10.1016/S0168-9002(00)00745-2)
- [48] Kolotov, V.P., Atrashkevich, V.V. and Gelsema, S.J. (1996) Estimation of True Coincidence Corrections for Voluminous Sources. *Journal of Radioanalytical and Nuclear Chemistry*, **210**, 183-196. <https://doi.org/10.1007/BF02055417>
- [49] Strom, E. and Israel, H.I. (1970) Photon Cross Sections from 1 keV to 100 MeV for Elements  $Z = 1$  to  $Z = 100$ . *Atomic Data and Nuclear Data Tables*, **7**, 565-681. [https://doi.org/10.1016/S0092-640X\(70\)80017-1](https://doi.org/10.1016/S0092-640X(70)80017-1)
- [50] Wickens, T.D. (2002) *Elementary Signal Detection Theory*. Oxford University Press, New York. <https://doi.org/10.1093/acprof:oso/9780195092509.001.0001>